PAPER

Experimental Determination of Propagation Paths for the ETC System—Equipment Development and Field Test—

Katsuyuki HANEDA[†a)], ***Student Member***, **Jun-ichi TAKADA**[†], **Takeo IWATA**[††], ***Members***, **Yoshitaka WAKINAKA**[†††], ***and*** **Takeshi KUNISHIMA**[††††], ***Nonmembers***

SUMMARY Electronic Toll Collection (ETC), an application of Dedicated Short Range Wireless Communication (DSRC), had suffered from wrong operations due to multipath problems. To solve this problem, we proposed to apply a simple configured path determination scheme for the ETC system. The system consists of a vector network analyzer, low-noise amplifier, and X-Y positioner and achieves an automatic measurement of the spatial transfer function with emphasis on accurate measurement and reproducibility. For the reliable identification of the propagating paths, 3-D Unitary ESPRIT and SAGE algorithms were employed. Having developed the system, field experiments at the toll gate of the highway was carried out. In the measurements, we could determine many propagation paths so that the dominant propagation phenomena at the toll gate was identified. They included a ground-canopy twice reflected wave, which was a potential path that caused wrong operation. Consequently, their reflection coefficients and polarization characteristics were investigated. From the results, applicability of the path determination system for short range on-site measurement was confirmed.

key words: *ETC, DSRC, propagation, short range wireless communication, measurement system, path determination, 3-D unitary ESPRIT, SAGE algorithm*

1. Introduction

Recently, the demand for short range wireless communication is expanding such as in Intelligent Transport System (ITS), and wireless local area network (LAN). However, these systems often suffer from multipath and shadowing. In Japan, the ETC system had some problems in system operations due to the presence of unexpected multipath waves at the beginning of the deployment [1].

ETC is a communication system between a roadside antenna at the toll gate and a vehicular antenna inside the car. In this system, the waves reflected, diffracted or shadowed by the canopy, booth, road surface and cars may cause problems to its own or the following cars because they may extend the coverage area of the system. In the initial measurement at the toll gate [1], the ground and canopy twice reflected waves as shown in Fig. 1 were identified as the suspicious waves that caused the problem. A car that passes through the toll gate receives both direct wave and ground-canopy reflected wave at different points, so toll payment may occur twice. Another reported trouble was that the exit bar did not open and the car that was passing through the gate bumped it. In this context, further needs to investigate the potential reflected paths with respect to their power and polarization has arose. It seems that this kind of problem occured due to the system design based only on line-of-site (LOS) paths.

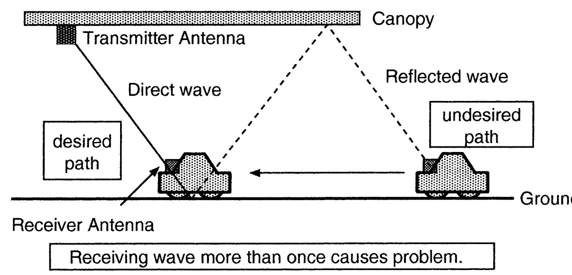

Fig. 1 Multipath problem of ETC occured at the beginning of deployment.

For this purpose, it was necessary to specify the waves which caused the problem. We can suppress the undesired waves by putting an electromagnetic absorber at the reflection point of the wave. Moreover, after putting the electromagnetic absorber, its peformance evaluation is crucial for the maintainance and sustainable usage of the toll gate. Such a kind of inspection is achieved only by on-site measurements with path determination systems. Therefore, what we proposed here is an application of a conventional channel sounding scheme as a path determination system for the improvement of the ETC/DSRC system.

There have been many studies on the development of propagation channel estimation techniques and channel sounders (e.g., [2]–[4]). However a channel sounder requires a complex hardware design, so some simple system is preferable when we consider the development time and cost. Therefore, a channel measurement system with a simple configuration is employed in this study. The system integrates some off-the-shelf measurement equipments such as a vector network analyzer (VNA), X-Y positioner, and PC for simultaneous direction of arrival (DOA) and time of arrival (TOA) estimation. There have been many channel

Manuscript received January 8, 2004.
Manuscript revised May 9, 2004.
Final manuscript received July 20, 2004.
[†]The authors are with the Department of International Development Engineering, Tokyo Institute of Technology, Tokyo, 152–8552 Japan.
[††]The author was with the Japan Public Highway Corporation, Tokyo, 100-8979 Japan. Presently, with the Highway Industry Development Organization.
[†††]The author was with Takenaka Corporation, Chiba-shi, 270-1395 Japan. Presently, with Koseyu Corporation.
[††††]The author is with Takenaka Corporation, Chiba-shi, 270–1395 Japan.
a) E-mail: haneda@ap.ide.titech.ac.jp

measurement campaigns by using a VNA, with superresolution techniques [5], [6], with synthesized array antennas [6]–[8], with real antenna arrays [9] and for millimeter-wave propagation measurements [10]. Based on their studies, we developed an improved system which focuses on the precise measurements with reproducibility and accurate estimation of signal parameters.

An experiment at the toll gate of the highway was carried out with the use of this path determination system. In the results, several propagation paths were observed which included the ground-canopy twice reflected wave. The estimated paths could be identified to the physical structure of the environments, i.e. canopy, ground, polls at the toll as well as the direct wave so that validity of the on-site measurement with our system was confirmed. Consequently, detailed investigations on the reflection coefficients, polarization characteristics and dominant scatteres were examined.

This paper consists of the following sections: the next section describes the specification of the path determination system and in Sect. 3, a brief information on the signal processing is given. Section 4 presents the result of the experiment at the toll gate of the highway and the conclusion is given in Sect. 5.

2. Specification of Path Determination System

The system we developed in this research is depicted in Fig. 2. This system has two characteristics:

- It can measure the spatial transfer function automatically while retaining accuracy.
- It offers precise estimation of the parameters by using high resolution algorithms.

In Fig. 2, one of the antenna apertures is a synthesized uniform rectangular array (SURA) which is realized by scanning a single antenna element spatially by the aid of a X-Y positioner. This allows us to avoid the complex calibration procedure due to the mutual coupling of the antenna array. The configuration of the antenna aperture is arbitrary

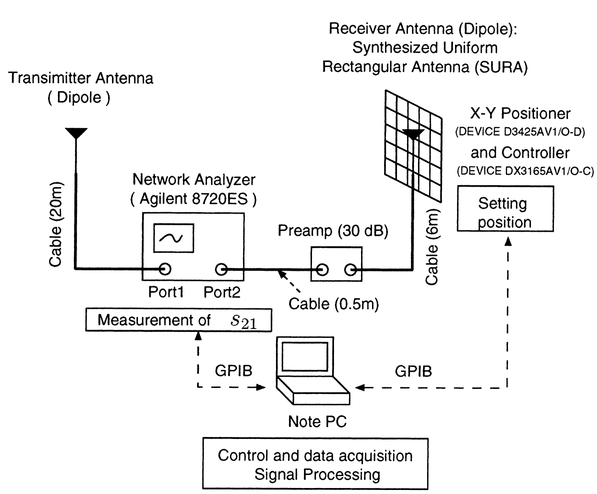

Fig. 2 Path determination system.

and depends on the antenna positioning equipment. The use of a low-noise amplifier enables us to extend the dynamic range of the signal to be detected.

Taking into account that it takes much time to move antennas and some accuracy is required in antenna alignment, we automated this system with respect to controlling the X-Y positioner and VNA via GPIB. This drastically reduces the measurement time while retaining the accuracy of antenna alignment of 1 [mm]. The maximum size of the antenna aperture is 2.42 [m] × 1.5 [m] in either vertical or horizontal plane. This system is shown to derive reliable results for time-invariant channels while retaining reproducibility.

3. Parameters Estimation Schemes

In order to estimate the parameters of the incident waves from the transfer function measured at the VNA, we used the 3-D Unitary ESPRIT in conjunction with the SAGE algorithm which achieves higher resolution than Fourier Transform (Beam Forming Method).

3.1 3-D Unitary ESPRIT

ESPRIT (Estimation of Signal Parameters via Rotational Invariance Technique) [11] is an algorithm based on the eigenspace analysis. In physical terms, it is equivalent to finding out the parameters of the incident waves by using the phase difference between groups of uniformly positioned elements such as an uniform linear array antenna input. Unitary ESPRIT [12] has an advantage in computaional speed compared to the conventional ESPRIT and can expand to multi-dimensional simultaneous parameters estimation [13]. In our system, 3-D Unitary ESPRIT is considered [2]. However, the algorithm may have an insufficient performance when it is applied to short range wireless communication environment due to the following aspects:

- **Correlation of the incident waves/estimation of the number of waves and the number of measurement points:**
  In multipath environments, superimposed signals often arrive coherently with each other, and it is required to reduce the coherence by introducing a smoothing preprocessing in the algorithm [14]. However, it comes to light from the experiment that we cannot reduce it perfectly because the coherency is too strong. In this case, there may exist some waves detected degenerately which should have been separately detected. This phenomenon can cause a bias in the parameter estimation result, thus the estimation of the number of waves is essential in the process.

  If incident waves are incoherent with each other, the number of waves are equal to the number of eigenvalues that are larger than noise power. In case of the estimation of coherent waves, however, that criteria does not hold. The same phenomenon can be seen even when we introduce spatial smoothing as preprocessing. Although there is an approach from the information theoretical point of view that estimates the number of waves called MDL [15], the result is not always so reliable. In present conditions, we only assume the validity of each result obtained by changing the number of waves.

In addition, the upper limit of the number of waves we can estimate depends on a dimension of the correlation matrix for reasons indicated above as well as the change of the resolution. And the dimension of the correlation matrix is also dependent on the number of measurement points. Therefore when we determine the number of measurement points, we must consider the upper limit of the incident waves and the way of smoothing.

- **Plane wave approximation:**
In short range wireless communication environment, there may exist a wave that does not satisfy the plane wave approximation which is a hypothesis of this algorithm. Thus we must consider other methods for estimation of these waves.

These kinds of phenomena often cause erroneous estimation results, especially in the form of spurious ray paths which are unable to be identified in the real environment.

3.2 SAGE Algorithm

To improve the defects of 3-D Unitary ESPRIT listed above, we propose to use the SAGE algorithm [16] at the same time. This algorithm is essentially based on the maximum likelihood estimation (MLE) which is statistically an optimum estimator. The SAGE algorithm reduces the computatioal cost compared to the MLE by exploiting hidden data spaces [17], while retaining accuracy. However, we must bear in mind that the result of the SAGE algorithm is not always a global optimum solution, thus the initial value of the search is very important. There is a way that generates the initial value called succesive interference cancellation [16], but in this system the result of 3-D Unitary ESPRIT is employed as an initial condition [18]. By using this scheme, it is expected to reduce the effect of spurious paths.

3.3 Resolution and Accuracy of the Parameters Estimation

Considering the structure of the toll gate, we assumed that it is enough to achieve resolution of spatially 10 [deg] and 15 [ns] in temporal domain to distinguish the dominant propagation paths. They correspond to the electrical aperture size of 4.5λ and frequency band of 67 [MHz] with respect to the Fourier resolution. They were achieved in the field experiment at the toll gate of the highway, whose specifications and results are described in Sect. 4. Concerning the accuracy of the estimation, root mean square error (RMSE) of the results were about 0.23 [deg] in the angle, and 0.15 [ns] in the delay domain, respectively. RMSE of the estimated complex amplitude was 0.25 [dB] and 16 [deg] with respect to the magnitude and phase. The RMSE was obtained by using the Monte-carlo simulation of ESPRIT and SAGE in which the detected waves were successfully resolved either in the DOA or TOA domain. In the simulation, signal-to-noise ratio (SNR) of the wave was 20 [dB] and plane wave incidence was assumed.

4. Field Experiment at a Toll Gate of the Highway

We carried out a field measurement at a toll gate of a highway. The scenario of the measurement was the third lane of Hinode toll gate in Center District Highway at Tokyo, Japan. In the lane, we executed the measurements twice at different points. Note that this toll gate had already been designed to supress the multipath waves from the beginning so that we changed the position of the transmitter antenna (Tx) and the receiver antenna (Rx) intentionally in order to observe multipath propagation. During the measurement, there were no cars passing by and no moving objects around the field, thus we can assume the environment to be time invariant. The details of the parameters of the measurement and signal processing are listed in Table 1.

We employed dipole antennas at Tx and Rx, thus linearly polarized waves were used in the measurement. In this case, the resolution characteristics of the superimposed signals were dependent on the polarized direction of the waves, i.e., in horizontally polarized case and vertically polarized case, because of the directivity of the dipole antenna. Consequently, we exploited polarization averaging in ESPRIT [19] which takes advantage of this nature so that stable resolution in angle estimation is expected. In SAGE algorithm, the search was conducted for both polarizations simultaneously. Then we can estimate the polarization dependent gain

Table 1 Specifications of the measurement and signal processing.

Measurement points	Spatially 10×10 points (Vertical plane, interval 25 [mm]) 21 points over frequency from 5.8 [GHz] to 5.9 [GHz].
Estimated Parameters	The number of paths/azimuth, elevation, delay and complex amplitude of each path.
Antennas	Dipole antennas at both Tx and Rx. Reflection coefficient is below −10 [dB] in 5.8–5.9 [GHz].
Calibration	Back-to-back at the distance between Tx and Rx of 1 [m] in an open space.
Snapshot	20 times.
Signal Processing	LS 3-D Unitary ESPRIT (initial value estimation), SAGE algorithm.
Smoothing in ESPRIT	Spatially 4 times and 7 times over frequency.
Wave Polarization	Vertical-Vertical, Horizontal-Horizontal (with polarization averaging in ESPRIT, simultaneous search for both polarization in SAGE).
Signal-to-Noise Ratio	Approx. 40 [dB].

of a path. With the use of a LNA, the SNR at the input of the VNA was estimated to be approximately 40 [dB].

Here we show the method of system calibration, the test environment, and the results obtained by using the SAGE algorithm which employed the result of 3-D Unitary ESPRIT as an initial condition.

4.1 Calibration of the System

When we measured the distribution of the transfer function spatially by using the proposed system, VNA also measured the transfer function of cables and amplifier simultaneously which was not negligible so that it is required to remove them from measured data. This process is refered to as calibration.

In the system depicted in Fig. 2, suppose that the transfer functions of free space and the system are denoted by $H(f)$ and $G(f)$, respectively. If we can neglect the reflection within the equipment, transfer function $X(f)$ measured by VNA is expressed as

$$X(f) = H(f) \times G(f). \tag{1}$$

Here, if $H(f)$ is expressed as a Friis' free space transmission formula

$$H(f) = \frac{\lambda}{4\pi d} \exp\left(-\mathrm{j}\frac{2\pi}{\lambda}d\right), \tag{2}$$

we can derive the transfer function of the system $G(f)$ from the measured data $X(f)$ through equation (1). Here λ is the wavelength and d is the distance between Tx and Rx. We estimate $G(f)$ by a back-to-back calibration procedure and regard $G(f)$ as the calibration data. In the experiment, the transfer function of free space can be extracted by dividing the measured data from VNA by $G(f)$.

4.2 Results in Scenario A

Scenario A is depicted in Fig. 3. The transmitter antenna was set to 4.79 meters high by a crane below the ETC gate. And the receiver antenna is depicted at the center of the spatial scanning.

The estimation results in scenario A are presented in Table 2 and the ray paths identified are depicted in Fig. 3. Definition of the angles is also described in the figure. Path determination was achieved with the use of DOAs and TOAs. First, DOAs were used to specify the reflection point so that the exact path can be determined in the environment. After that, TOA was examined whether it agreed with the TOA derived from the length of specified path or not. If they indicate different values, the path is regarded as a spurious path.

In the result of ESPRIT, several spurious paths appeared. For example, a wave whose path parameters are azimuth 5.7 [deg], elevation −51.9 [deg] and delay 18.7 [ns], were assumed to be incident from ground but its delay time was much smaller than the one derived from the path length, 25.8 [ns]. However, after the processing of SAGE, the delay time was refined so that exact path determination to the ground reflected wave was accomplished (#2 of Table 2). As a result, results from SAGE algorithm were free from the spurious paths.

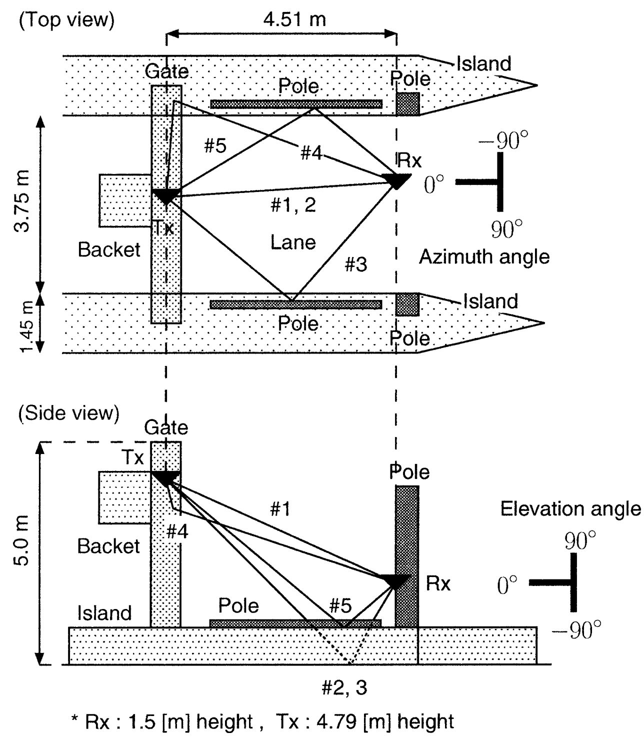

Fig. 3 Ray path identification at scenario A.

Table 2 Estimated parameters of incident waves at scenario A: theoretical values are shown in ( ) for direct wave and specular reflected waves.

Reflection Point	Azimuth [deg]	Elevation [deg]	Delay [ns]	Gain [dB]	Phase [deg]
#1 (Direct Wave)	2.5 (5.1)	34.6 (36.0)	18.6 (18.7)	v:0.0 h:0.0	v:0 h:0
#2 Ground	1.9 (5.1)	−55.3 (−54.3)	26.0 (25.8)	v:−12.9 h:−9.3	v:225 h:348
#3 Ground and Left Poll	32.9	−55.1	31.2	v:−30.5 h:−15.6	v:25 h:134
#4 Right Gate	−22.6	23.9	27.2	v:−22.6 h: noise	v:116 h: noise
#5 Right Poll	−58.3	−13.1	29.3	v:−19.7 h:−34.4	v:149 h:269

In Table 2, estimates of the parameters by geometical optics are also shown for the specular paths. The complex amplitude of each path is normalized by the first arrival wave and is expressed in the form of gain and phase. v and h mean path gain values of vertically polarized wave and horizontally polarized wave respectively. The expression "noise" represents that the path was not able to be detected because the received power was below noise level.

According to the results, we were able to detect 5 paths in this scenario. For the specular reflected waves (#1: direct wave and #2: ground reflected wave), the results well matched the theoretical ones. We can see 3 non-specular reflected waves whose gain were at least 10 [dB] below the direct path. Wave #3 experiences reflection on the ground and diffraction at the poll equipped at the left side of the road. Wave #4 is a diffraction from the edge of the gate and wave #5 is a diffraction from the poll equipped at the right side of the road.

4.3 Results in Scenario B

Scenario B is depicted in Fig. 4 as well as the definition of the angles. The transmitter antenna was set to 5.0 meters high by crane and the receiver antenna was placed at the center of the spatial scanning. The estimation results in scenario B is presented in Table 3 and the identified ray paths are depicted in Fig. 4. In this scenario, spurious paths also appeared, e.g., the wave with azimuth −1.8 [deg], elevation 44.2 [deg] and delay time 28.5 [ns] which corresponds to the reflection from the canopy, but delay time was not consistent with the length of specified path, 23.1 [ns]. However, after refinement of the result by SAGE, it converged to the direct wave (#1 of the Table 3). We observed no spurious paths in the result of SAGE.

In this scenario, 7 waves were detected because there were more objects around it than scenario A and it arose from the beam, pole, canopy and ground reflection. We could also see ground-canopy twice reflected wave which might cause an undesired extension of the coverage area in

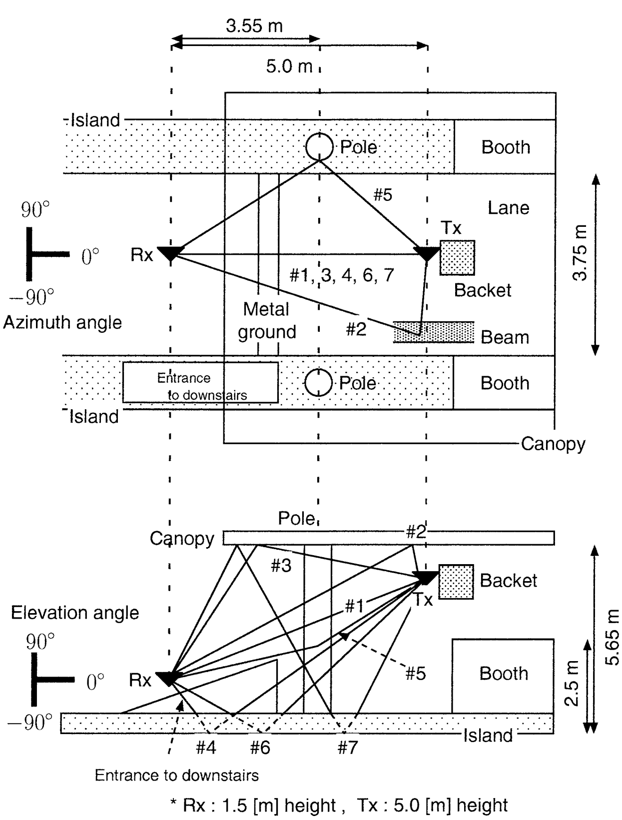

Fig. 4 Path identification at scenario B.

communication. Note that non-specular waves are dominant among reflected waves. One reason is the shape of the objects, i.e. cylindrical poll, corrugated canopy. Non-specular scattering from the metals equipped on the ground was detected (#6) as well as the specular paths from the ground (#4). For the parameters of specular reflected waves, we could see close agreement with the theoretical values.

4.4 Discussion on the Dominant Propagation Phenomena

From the experiments, dominant propagation paths were discovered. They are scattering at

- Ground,
- Canopy (including beams),
- Polls equipped at the roadsides.

Among them, ground and canopy scattering consist of specular reflection which can be easily predicted intuititively, while scattering at the poll is normally non-specular reflection or diffraction because of the shape of the poll. Note that metal parts in the ground can also produce an enhanced reflection even though it is a non-specular direction.

In order to predict the incident power of the scattering wave, reflection coefficients are calculated for each path in scenarios A and B. The results are shown in Tables 4 and 5, respectively. For the specular reflected waves, they are compared to the theoretical ones. In the theoretical derivation, the reflection plane is assumed to be semi-infinite and have a finite thickness of 10 [cm]. The permittibity of reflection plane is $\varepsilon_r = 7.0 - j0.85$ [20], which is adequate for asphalt. Perfect refletion is assumed in canopy for the twice reflected waves in scenario B (#7), since the canopy is made of metal although it is corrugated. From the results it can be observed that theoretical consideration can be applicable for predicting scattering loss of the specular reflected waves, i.e. ground and canopy reflection. For the reflection coefficients of non-specular waves, they indicate larger loss than those

Table 3 Estimated parameters of incident waves at scenario B: theoretical values are shown in ( ) for direct wave and specular reflected waves.

Reflection point	Azimuth [deg]	Elevation [deg]	Delay [ns]	Gain [dB]	Phase [deg]
#1 (Direct wave)	3.9 (2.3)	37.9 (35.0)	19.6 (20.4)	v:0.0 h:0.0	v:0 h:0
#2 Right Beam	−25.3	27.4	26.1	v:−20.2 h:−19.8	v:70 h:253
#3 Canopy	2.1	67.6	25.9	v:−13.6 h:−13.8	v:88 h:211
#4 Ground	2.4 (2.3)	−59.5 (−52.4)	27.5 (27.3)	v:−11.2 h:−10.6	v:191 h:304
#5 Left Poll	37.4	20.4	29.2	v:−11.9 h:−21.2	v:218 h:257
#6 Ground (Metal part)	4.2	−39.9	36.0	v:−33.6 h:−12.5	v:200 h:286
#7 Ground and Canopy	2.8 (2.3)	72.8 (71.3)	50.9 (52.1)	v: noise h:−16.1	v: noise h:239

Table 4 Reflection coefficients of each path in scenario A: theoretical values are shown in ( ) for the specular reflected waves.

Path	Ref. coeff. [dB] Vertical wave	Ref. coeff. [dB] Horizontal wave
#2 (Ground)	−10.0 (−8.3)	−6.5 (−5.7)
#3 (Ground & Poll)	−26.1	−11.1
#4 (Gate)	−19.3	Not detected
#5 (Poll)	−15.8	−30.5

Table 5 Reflection coefficients of each path in scenario B: theoretical values are shown in ( ) for the specular reflected waves.

Path	Ref. coeff. [dB] Vertical wave	Ref. coeff. [dB] Horizontal wave
#2 (Beam)	−17.7	−17.3
#3 (Canopy)	−11.2	−11.3
#4 (Ground)	−8.3 (−8.0)	−7.7 (−5.9)
#5 (Poll)	−8.4	−17.7
#6 (Ground)	−28.3	−7.0
#7 (Ground & Canopy)	Not detected	−7.8 (−6.6)

predicted by theoretical considerations. We could confirm the dependence of reflection coefficients on the polarization since vertical wave reflections have larger loss than that of horizontal waves.

4.5 Discussions on the Characteristics of Circular Polarization

Since the ETC system employs circular polarized waves, prediction of the propagation phenomena with respect to circular polarized wave would be necessary. The complete construction of circular polarized waves needs co- and cross-polarization measurement. In our field tests, however, sufficient SNR in the cross-polarization measurement was not accomplished so we could not collect reliable data. In other words, the effect of cross-polarization is negligible compared to the co-polarization in terms of the SNR. Therefore, considering only the co-polarization case is sufficient for reconstructing the circular polarized component.

Suppose pure right-handed circular polarized (RHCP) wave of unit power is radiated from Tx, polarimetric incident field at Rx is denoted as Eq. (3),

$$\begin{bmatrix} y_V \\ y_H \end{bmatrix} = \begin{bmatrix} r_{VV} & -\mathrm{j}r_{VH} \\ \mathrm{j}r_{HV} & r_{HH} \end{bmatrix} \begin{bmatrix} \frac{1}{\sqrt{2}} \\ \frac{\mathrm{j}}{\sqrt{2}} \end{bmatrix}, \quad (3)$$

where y_V is a received field with respect to the vertically polarized wave and y_H is that of horizontal polarization. The matrix composed of r expresses a scattering loss, including free space attenuation. The diagonal elements denote scattering coefficients for the vertical and the horizontal polarization, while the non-diagonals represent polarization rotation effects. Herein the non-diagonal elements can be treated as zero, since they are negligibly small. Obtained y_V and y_H enables us to analyze the incident power of RHCP and left-handed circular polarized (LHCP) waves for each path. Note that y_V and y_H should be normalized by a definition of the notation of circular polarized waves such that y_V is a reference of phase. For example, in wave #2 of scenario A, the received field is $y_V = 0.1601$, $y_H = -0.2033 - \mathrm{j}0.1320$ and it corresponds to an elliptic wave. Any elliptic wave can be decomposed into the RHCP and LHCP waves then the received field yields −16.8 [dB] and −12.0 [dB] of the RHCP and LHCP components, respectively. The power denotes a relative value, which is normalized by the received power of the RHCP of the direct wave. It is observed that the LHCP component more or less appears even when pure RHCP wave is radiated. This is due to the different propagation characteristics between vertical and horizontal waves. They lead to the degradation of axis ratio of circular polarized waves, which result in the elliptic polarized waves. Incident power of the RHCP and LHCP for other paths are shown in Table 6 and Table 7.

Table 6 Normalized incident power of the RHCP and LHCP in scenario A: when pure RHCP wave is radiated.

Path	Power of RHCP [dB]	Power of LHCP [dB]
#1 (Direct wave)	0.0	−∞
#2 (Ground)	−16.8	−12.0
#3 (Ground & Poll)	−22.0	−21.0
#4 (Gate)	−28.6	−28.6
#5 (Poll)	−26.4	−24.9

Table 7 Normalized incident power of the RHCP and LHCP in scenario B: when pure RHCP wave is radiated.

Path	Power of RHCP [dB]	Power of LHCP [dB]
#1 (Direct wave)	0.0	−∞
#2 (Beam)	−49.2	−20.0
#3 (Canopy)	−20.1	−14.8
#4 (Ground)	−16.1	−12.5
#5 (Poll)	−15.8	−20.3
#6 (Ground)	−18.4	−18.6
#7 (Ground & Canopy)	−22.1	−22.1

5. Conclusion

In this paper, propagation environments of the ETC system were investigated with a simple configurated path determination system and advanced parameters estimation algorithms. The system is easily integrated with commercial equipments, VNA, X-Y positioner and PC and achieves a completely automated measurement. The accuracy of antenna alignment and reproducibility were emphasized in the system design. The use of SAGE algorithm in conjunction with 3-D Unitary ESPRIT makes it possible to reduce the spurious paths.

The measurement results at the toll gate of the highway showed that the measurement system could determine many propagation paths in the environment. They included the ground-canopy twice reflected wave which caused an incorrect operation in the ETC. Consequently, their scattering coefficient as well as the polarization characteristics were analyzed.

The validity of the path determination system were confirmed by the experiment so that several applications can be undertaken in addition to the undesired path detection: efficiency evaluation of the electromagnetic absorber at the toll gate, coverage design in DSRC (ex. road to vehicle communication). Such a kind of analysis is accomplished only by the on-site measurement, then the possibility to contribute to those works by the path determination system can be emphasized. This system can be applied not only to ITS, but also to other short range communications, link design and performance evaluation of indoor wireless LAN and Ultra Wideband (UWB) system by employing the horizontal spatial scanning [21], [22].

Acknowledgement

The authors would like to thank Kei Sakaguchi from Tokyo Institute of Technology for helping a lot in our research. And we want to express our gratitude to Japan Highway Public Corporation for preparation of the experiment at the toll gate.

References

[1] T. Iwata, Y. Wakinaka, and J. Takada, "Experimental identification of undesired propagation paths for ETC," Proc. 2nd International Workshop on ITS Telecommunications (ITST2001), pp.131–136, Yokosuka, Japan, Oct. 2001.

[2] K. Sakaguchi, J. Takada, and K. Araki, "A novel architecture for MIMO spatio-temporal channel sounder," IEICE Trans. Electron., vol.E85–C, no.3, pp.436–441, March 2002.

[3] K. Kalliola, H. Laitinen, L.I. Vaskelainen, and P. Vainikainen, "Real-time 3D spatial-temporal dual-polarized measurement of wideband radio channel at mobile station," IEEE Trans. Instrum. Meas., vol.49, no.2, pp.439–448, April 2000.

[4] R.S. Thomä, D. Hampicke, A. Richter, G. Somerkorn, A. Schneider, U. Trautwein, and W. Wirnitzer, "Identification of time-variant directional mobile radio channels," IEEE Trans. Instrum. Meas., vol.49, no.2, pp.357–364, April 2000.

[5] H. Yamada, H. Ohmiya, Y. Ogawa, and K. Itoh, "Superresolution techniques for time domain measurements with a network analyzer," IEEE Trans. Antennas Propag., vol.39, no.2, pp.177–183, Feb. 1991.

[6] K. Sakaguchi, J. Takada, and K. Araki, "On measuring the delay profile and the direction of arrival by using super resolution algorithm," Proc. 1998 IEEE Veh. Technol. Conf. (VTC '98), pp.154–158, May 1998.

[7] H. Suzuki and A.S. Mohan, "Measurement and prediction of high spatial resolution indoor radio channel characteristic map," IEEE Trans. Veh. Technol., vol.49, no.4, pp.1321–1333, July 2000.

[8] N. Kikuma, T. Kitamura, M. Ogawa, and N. Inagaki, "Signal parameters estimation of indoor multipath waves with triangular antenna array," Proc. Int. Symp. on Antenna and Propagation 1992 (ISAP1992), vol.2, pp.675–679, Sapporo, Japan, Sept. 1992.

[9] R.D. Tingley and K. Pahlavan, "Space-time measurement of indoor radio propagation," IEEE Trans. Instrum. Meas., vol.50, no.1, pp.22–31, Feb. 2001.

[10] T. Manabe and T. Ihara, "Propagation studies at 60 GHz for millimeter-wave indoor communication systems," J. Commun. Res. Lab., vol.41, no.3, pp.167–174, Nov. 1994.

[11] R. Roy and T. Kailath, "ESPRIT—Esimation of signal parameters via rotational invariance techniques," IEEE Trans. Acoust. Speech Signal Process., vol.37, no.7, pp.984–995, July 1989.

[12] M. Haardt and J.A. Nossek, "Unitary ESPRIT: How to obtain increased estimation accuracy with a reduced computational burden," IEEE Trans. Signal Process., vol.43, no.5, pp.1232–1242, May 1995.

[13] M. Haardt and J.A. Nossek, "Simultaneous schur decomposition of several nonsymmetric matrices to achieve automatic pairing in multidimensional harmonic retrieval problems," IEEE Trans. Signal Process., vol.46, no.1, pp.161–169, Jan. 1998.

[14] T.J. Shan, M. Wax, and T. Kailath, "On spatial smoothing for direction-of-arrival estimation of coherent signals," IEEE Trans. Acoust. Speech Signal Process., vol.ASSP–33, no.4, pp.806–811, Aug. 1985.

[15] M. Wax and T. Kailath, "Detection of signals by infomation theoretic criteria," IEEE Trans. Acoust. Speech Signal Process., vol.ASSP–33, no.2, pp.387–392, April 1985.

[16] B.H. Fleury, M. Tschudin, R. Heddergott, D. Dahlhaus, and K.I. Pedersen, "Channel parameter estimation in mobile radio environments using the SAGE algorithm," IEEE J. Sel. Areas Commun., vol.17, no.3, pp.434–449, March 1999.

[17] J.A. Fessler and A.O. Hero, "Space-alternating generalized expectation-maximization algorithm," IEEE Trans. Signal Process., vol.42, pp.2664–2677, Oct. 1994.

[18] M. Tschudin, R. Heddergott, and P. Truffer, "Validation of a high resolution measurement technique for estimating the parameters of impinging waves in indoor environments," Proc. Personal Indoor and Mobile Radio Communications 1998 (PIMRC '98), pp.1411–1416, Boston, MA, Sept. 1998.

[19] H. Yamada, M. Yoshino, and Y. Yamaguchi, "Resolution enhancement of the MUSIC algorithm with wave polarization," Proc. 4th International Workshop on Radar Polarimetry, pp.87–95, Nantes, France, July 1998.

[20] Rec. ITU-R P. 1238, "Propagation data and prediction models for the planning of indoor radiocommunication systems and radio local area networks in the frequency range 900 MHz to 100 GHz," ITU-R Recommendations, vol.1997, P Series-Part 2, pp.252–261, ITU, Geneva, 1998.

[21] K. Haneda and J. Takada, "High resolution estimation of NLOS indoor MIMO channel with network analyzer based system," Proc. Personal Indoor and Mobile Radio Communication 2003 (PIMRC2003), vol.1, pp.675–679, Beijing, China, Sept. 2003.

[22] K. Haneda and J. Takada, "An application of SAGE algorithm for UWB propagation channel estimation," Proc. IEEE Conf. Ultra Wideband Systems and Technologies 2003 (UWBST2003), pp.483–487, Reston, VA, Nov. 2003.

Katsuyuki Haneda was born in Kanagawa, Yokohama, Japan in 1979. He received the B.E. and M.E. degrees from Tokyo Institute of Technology, Japan in 2002 and 2004, respectively. His current interests are wireless propagation and channel modelling, array signal processing, ultra-wideband radio, and conservation and development of World Heritage Sites through engineering. He is a student member of IEEE.

Jun-ichi Takada was born in Tokyo, Japan in 1964. He received the B.E., M.E., and the D.E. degrees from Tokyo Institute of Technology, Japan, in 1987, 1982, respectively. From 1992 to 1994, he has been a Research Associate Professor at Chiba University, Chiba, Japan. From 1994, he has been an Associate Professor at Tokyo Institute of Technology, Tokyo, Japan. His current interests are wireless propagation and channel modelling, array signal processing, and ultra-wideband radio. He received the Excellent Paper Award and Young Engineer Award from IEICE, Japan, in 1993 and 1994, respectively. He is a member of IEEE and ACES.

Takeo Iwata was born in Gifu, Japan in 1948. He is a professional in the radio wave communication field since being employed by the Japan Highway Cooperation in 1967, working up from assistant manager to the chief of the laboratory. His current responsiblities include parking pricing system, ETC, VICS, and Smart Communication systems, and he is spearheading the emerging ITS development activity for the future. He is now manager of HIDO, the leading organization of ITS R&D. He is a member of IPSJ.

Yoshitaka Wakinaka was born in Osaka, Japan in 1966. He received the B.E., and M.E. degrees from Kansai University, Osaka, Japan, 1990, 1992, respectively. From 1992 to 2003, he had been a researcher at Takenaka Corpration. He is currently a president at Koseyu Corporation, Hyogo, Japan.

Takeshi Kunishima was born in Tokyo, Japan in 1963. He received the B.E degree from Nihon university science & technology, Japan in 1986. He has been a researcher of Takenaka road Construction since 1986. His current interest is development of electromagnetic absorbing pavement.